A NUMERICAL STUDY ON JET IMPINGEMENT OF PULSED PLASMA DISCHARGE ON A FLAT PLATE

K. Kim,[1] H.S. Kwak[1] and J.Y. Park*[2]

벽면에 충돌하는 펄스 플라즈마 제트 유동특성에 대한 수치적 연구

김 경 진,[1] 곽 호 상,[1] 박 중 윤*[2]

In this study, time-dependent numerical analysis was carried out to investigate the plasma jet impingement on a flat plate, and a compressible form of two-dimensional inviscid gas dynamics equations were solved using the flux corrected transport algorithm. The mathematical modeling of Joule heating in the polycarbonate capillary bore and the mass ablation from the bore wall was incorporated in the numerical analysis and the series of computation was performed for three cases depending on the distance of the opposing plate from the capillary exit. The computational results reveal that the presence of the opposing plate does not affect the flow conditions inside the capillary when compared to the case of open-air plasma discharge. In the exterior region, the flow structure shows the typical supersonic underexpanded jet which consists of the strong Mach disk in front of the opposing plate and the barrel shock at the side of the jet. It is found that the shock evolution becomes more quasi-steady when the plate distance decreases. Also, the effects of the distance between the capillary bore exit and the opposing plate on the flow conditions along the opposing plate are investigated and the pressure variation on the plate shows more complicated interaction between the plasma discharge and the opposing plate when the location of plate becomes closer to the capillary exit.

Key Words : Electrothermal Gun, Plasma Discharge, Supersonic Underexpanded Jet, Jet Impingement

1. INTRODUCTION

An electrothermal gun is the device to produce a pulsed plasma discharge using high-magnitude electrical energy pulses. This device was originally developed to improve the combustion rate of the solid propellants for the acceleration of the projectile by high temperature, high-pressure, and high-velocity plasma jet as an alternative to the conventional chemical igniters[1-3] and it was recently investigated to be a possible candidate for electrothermal thruster in a satellite propulsion system[4]. Another application of the electrothermal gun could be for the production of novel materials such as ceramic and metal nanopowders or the thermal plasma spray coating[5,6].

The electrothermal gun employs the high power discharge of electrical energy to vaporize the solid materials of capillary bore and/or electrodes, and the ionized vapor of eroded material forms a dense plasma during the duration of a high current discharge. The plasma vapor then exits the open end of the bore to create a highly ionized external plasma jet into the open or closed chamber.

Nusca et al.[3] conducted experiments for the open-air plasma discharge which showed the typical formation of

Received: January 12, 2009, Revised: February 26, 2009,
Accepted: March 6, 2009.

1 정회원, 금오공과대학교 기계공학부
2 비회원, 금오공과대학교 기계공학부
* Corresponding author, E-mail: jypark@kumoh.ac.kr

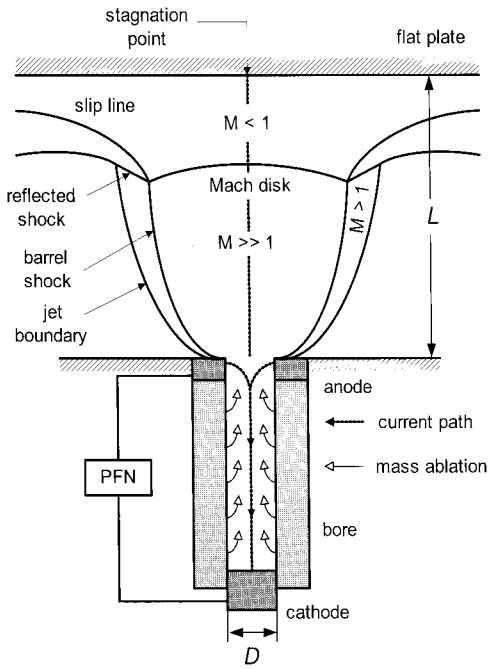

Fig. 1 Schematic diagram of electrothermal gun and the flow structure of plasma jet impinging on a flat plate

an underexpanded jet. Using the small-scale plasma igniter with polycarbonate liner, the open-air experiments were conducted to study the characteristics of the freely expanding plasma jet by Kohel et al.[7]. In the theoretical studies on the interior plasma conditions of electrothermal gun, there have been several different approaches depending on the degree of simplification. Powell and Zielinski[8] introduced a simple quasi-steady isothermal model and it provides excellent predictions despite its simplicity. Zaghloul et al.[9] and Kim[10] performed the theoretical analysis using time-dependent one-dimensional models. For the plasma discharge in the open-air, Nusca et al.[3] carried out numerical study by employing the time-dependent multidimensional CFD code, FAST3D. Kim[11] also studied the pulsed plasma discharge into the open-air by solving two-dimensional axisymmetric gas dynamics equations and his results showed good agreement with the plasma jet structure studied in the experiments by Kohel et al.[7].

This study presents the numerical simulation of the plasma discharge from electrothermal gun operations impinging on a flat plate by utilizing the time-dependent computation of gas dynamics in the two-dimensional axisymmetric domain that includes both interior and exterior of the electrothermal gun.

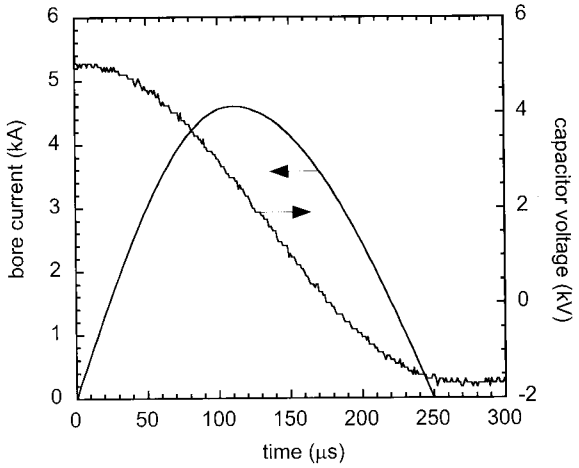

Fig. 2 Traces of recorded electrical current across the capillary bore and capacitor voltage during the electrothermal gun firing with the initial capacitor voltage of 5 kV[7]

2. Numerical Modeling

2.1 Electrothermal Gun

Fig. 1 shows a schematic diagram of the electrothermal gun which is driven by a pulse-forming network (PFN). PFN consists of the capacitor banks, inductors, resistors, and the ignition switch. When the discharge of stored electrical energy from the capacitor bank in PFN is initiated, the capillary bore and the fuse wire is establishing a current path between anode and cathode. Then the ablating polycarbonate bore material is subsequently vaporized and ionized due to intense Joule heating. The resulting plasma flow rapidly expands from an open end of the bore into the exterior region.

In this numerical study, the experimental work by Kohel et al.[7] provides the device dimensions and the operating conditions. The capillary bore of the electrothermal gun is 3.1 mm in diameter (D) and 30 mm in length, and made of polycarbonate (Lexan, $C_{16}H_{14}O_3$). The electrodes were made of copper-tungsten alloy to resist the material erosion from the plasma. A fine copper fuse wire was used between the anode and cathode to initiate the plasma discharge. The pulse forming network consists of 251 μF capacitor and 26 μH inductor and the energy initially stored in the capacitor bank was approximately 3.1 kJ with the initial capacitor voltage of 5 kV. Fig. 2 shows the recorded traces of the electrical current during the plasma discharge. The peak current of approximately 4.6 kA was obtained at the time of 110 μs,

and the pulse duration is approximately 250 μs.

The typical flow pattern of the freely expanding plasma discharge of high pressure from the capillary bore is a supersonic underexpanded jet, which is illustrated in Fig. 1. Due to the Joule heating from the electrical discharge and the mass addition from the bore wall, plasma flow velocity reaches sonic speed and the flow becomes choked at the bore exit. Mach disk is a nearly planar normal shock that resides in front of bore exit and its location depends on the pressure ratio of the bore exit to the background gas. The barrel shock forms at the side as the supersonic flow adjusts to the background state. The additional features include the hemispherical blast wave which propagates through the background gas and the expanding contact surface which divides the plasma and the background gas. This type of flowfield can be observed in some situations of impulsive supersonic jet such as gun muzzle blast[12]. Turbulent mixing could be considerable at the contact surface but it will not alter the inviscid nature of the shock structure substantially for the period of pulse duration.

2.2 Numerical Model

The time-dependent differential equations for conservation of mass, momentum (in radial and axial directions), and energy for the plasma flow are:

$$\frac{\partial \rho}{\partial t}+\frac{1}{r}\frac{\partial}{\partial r}(r\rho u_r)+\frac{\partial}{\partial z}(\rho u_z)=\dot{\rho}_a \tag{1}$$

$$\frac{\partial \rho u_r}{\partial t}+\frac{1}{r}\frac{\partial}{\partial r}(r\rho u_r^2)+\frac{\partial}{\partial z}(\rho u_r u_z)=-\frac{\partial P}{\partial r} \tag{2}$$

$$\frac{\partial \rho u_z}{\partial t}+\frac{1}{r}\frac{\partial}{\partial r}(r\rho u_r u_z)+\frac{\partial}{\partial z}(\rho u_z^2)=-\frac{\partial P}{\partial z} \tag{3}$$

$$\frac{\partial \rho \epsilon}{\partial t}+\frac{1}{r}\frac{\partial}{\partial r}(r\rho u_r \epsilon)+\frac{\partial}{\partial z}(\rho u_z \epsilon)=\frac{J^2}{\sigma} \tag{4}$$

$$\epsilon = e+\frac{1}{2}(u_r^2+u_z^2)+\frac{P}{\rho} \tag{5}$$

where ρ, P, u_r, u_z, and e are the mass density, pressure, radial velocity, axial velocity, and the specific internal energy, respectively. These equations represent the inviscid compressible gas dynamics. In the energy equation, the term in the right-hand side presents the Joule heating inside the capillary bore, where J is the current density and σ is the plasma electrical conductivity. The plasma specific internal energy consists of thermal energy, electronic energy, and chemical energy components such as

$$e=\frac{3}{2}(1+\alpha)\frac{kT}{\overline{m}}+e_{el}+e_{chem} \tag{6}$$

where α, k, and $\overline{m}$ are the degree of ionization, Boltzmann constant, and average particle mass of the heavy species, respectively. For the equation of the state, the following ideal gas approximation is considered:

$$P=(1+\alpha)\rho\frac{kT}{\overline{m}} \tag{7}$$

Because of high pressure and high temperature, the ablated material is fully dissociated into their elemental constituents and is partially or fully ionized. Also, at such extreme conditions, plasmas are expected to be in local thermodynamic equilibrium. Therefore, the equilibrium compositions of the plasma are determined by considering the following form of the Saha equation:

$$\frac{n_{i+1}n_e}{n_i}=2\frac{Q_{i+1}}{Q_i}\left(\frac{2\pi m_e kT}{h^2}\right)^{3/2}\exp\left(-\frac{I_i-\Delta I_i}{kT}\right) \tag{8}$$

where the subscripts i and i+1 represent a heavy species and its next ionization level and n_e is the electron number density. The partition functions Q_i can be determined by considering the degeneracy and the energy of electronic excitation level. The term ΔI_i is the correction to the ionization energy of heavy species I_i for the nonideal plasma behavior[10]. In this study, up to two ionization levels of the monoatomic heavy species are considered. For a partially ionized plasma, the electrical conductivity is determined based on the electron collisions with both neutral atoms and ions and can be expressed as

$$\sigma=\frac{n_e e_c^2}{m_e(\overline{\nu}_{en}+\overline{\nu}_{ei})} \tag{9}$$

where $\overline{\nu}_{en}$ is the electron-neutral collision frequency and $\overline{\nu}_{ei}$ is the electron-ion collision frequency. In evaluating $\overline{\nu}_{ei}$, Zollweg and Liebermann model[13] is implemented for a correction to the traditional Spitzer model to account for nonideal effects in a dense plasma. More details in the calculation of thermodynamic and transport properties of

polycarbonate plasma vapor can be found in the works of Batteh et al.[14] and Kim[10].

In order to model the mass ablation from the bore wall due to radiative heating from plasma column, the mass ablation density rate $\dot{\rho}_a$ is introduced in the mass equation as a source term. From the previous studies[8,10,11], the mass ablation is approximated by equating the radiative flux from the plasma to the interior wall of the capillary bore and the energy of the ablated material inside the bore. Therefore, $\dot{\rho}_a$ is given by

$$\dot{\rho}_a = \frac{4 f \sigma_{sb} T^4}{D \epsilon} \tag{10}$$

where σ_{sb} is the Stefan-Boltzmann constant and T is the temperature. In the above equation, the factor f represents the deviation of radiative flux from the blackbody behavior. Two source terms in mass and energy equations are applied only inside the capillary bore. Also, note that present study neglected the mass ablation from the electrodes and the explosion of the fuse wire. Aforementioned experiments[7] found that the fuse wire breaks down within 10 μs from initial current discharge and that the electrode mass loss is negligible.

2.3 Computational Procedure

The numerical scheme employed in this study is based on LCPFCT[15] which uses the one-dimensional flux-corrected transport (FCT) algorithm with fourth-order phase accuracy. This scheme is originally developed by Boris[16] and basically solves the generalized one-dimensional continuity equation in the form of

$$\frac{\partial \phi}{\partial t} + \frac{1}{r^{n-1}} \frac{\partial}{\partial r}(r^{n-1} \phi u) = \frac{1}{r^{n-1}} \frac{\partial}{\partial r}(r^{n-1} D_1) + C_2 \frac{\partial D_2}{\partial r} + D_3 \tag{11}$$

where ϕ is the generalized conserved quantity (ρ, ρ_p, ρu_r, ρu_z, $\rho \epsilon$) and the terms C_2, D_1, D_2, and D_3 accommodate the source terms. The integer n is 1 in axial direction and 2 in radial direction. This scheme has been proven to be highly accurate and efficient especially in resolving steep gradients and it can be easily extended to the two-dimensional cases by time step splitting in each spatial coordinate direction. A set of the governing equations in the previous section is separated into two sets for radial and axial coordinates and those two sets are subjected to successive integration along the corresponding directions at each time step.

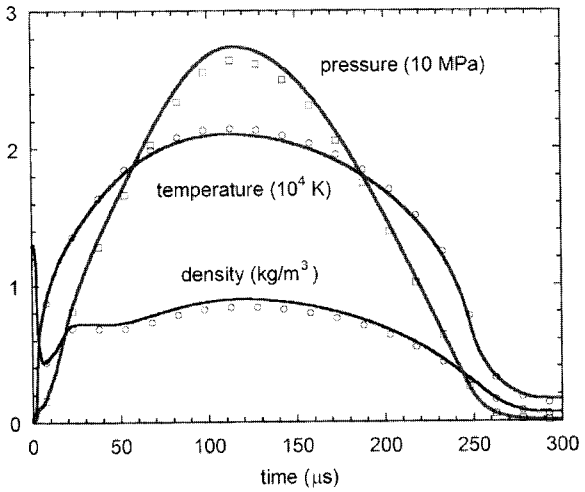

Fig. 3 Plasma conditions at the capillary bore exit. Solid lines are from the case of L/D = 5 and the symbols are from the case of open-air discharge

Axisymmetric computational domain includes the interior region of the capillary bore and the open-air region between the bore exit and the opposing plate. The plate surface is set to be thermally insulated and non-reacting with the impinging plasma discharge. The number of grid points in the computational domain is approximately 150,000 and the domain expands up to 25 bore diameters in radial direction. Note that the grids are clustered around the bore exit and near the plate surface to resolve the steep gradients. The initial condition of the computation is set to be the quiescent air at the standard atmospheric conditions and the integrating time step is determined by the CFL condition.

3. Results and Discussion

A series of numerical computations are carried out for three cases where the location of a opposing plate is 3, 5, and 10 bore diameters from the bore exit (L/D = 3, 5, 10). Fig. 3 shows the temporal variation of the calculated plasma conditions at the center of the capillary bore exit plane for the case of L/D = 5, compared with the case of open-air discharge from the previous study[11]. While the plasma properties show the maximum values at the time of peak current (110 μs), the comparison reveals that the presence of the plate in front of the plasma discharge does not affect the plasma conditions at the bore exit

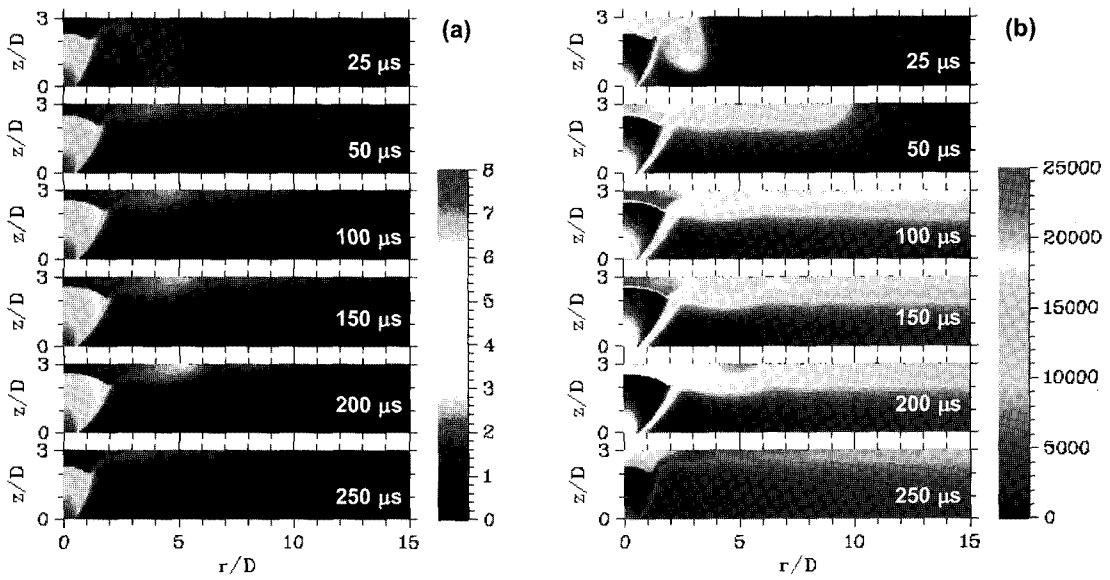

Fig. 4 Transient evolution of (a) Mach number and (b) temperature (in K) contours for the case of L/D = 3

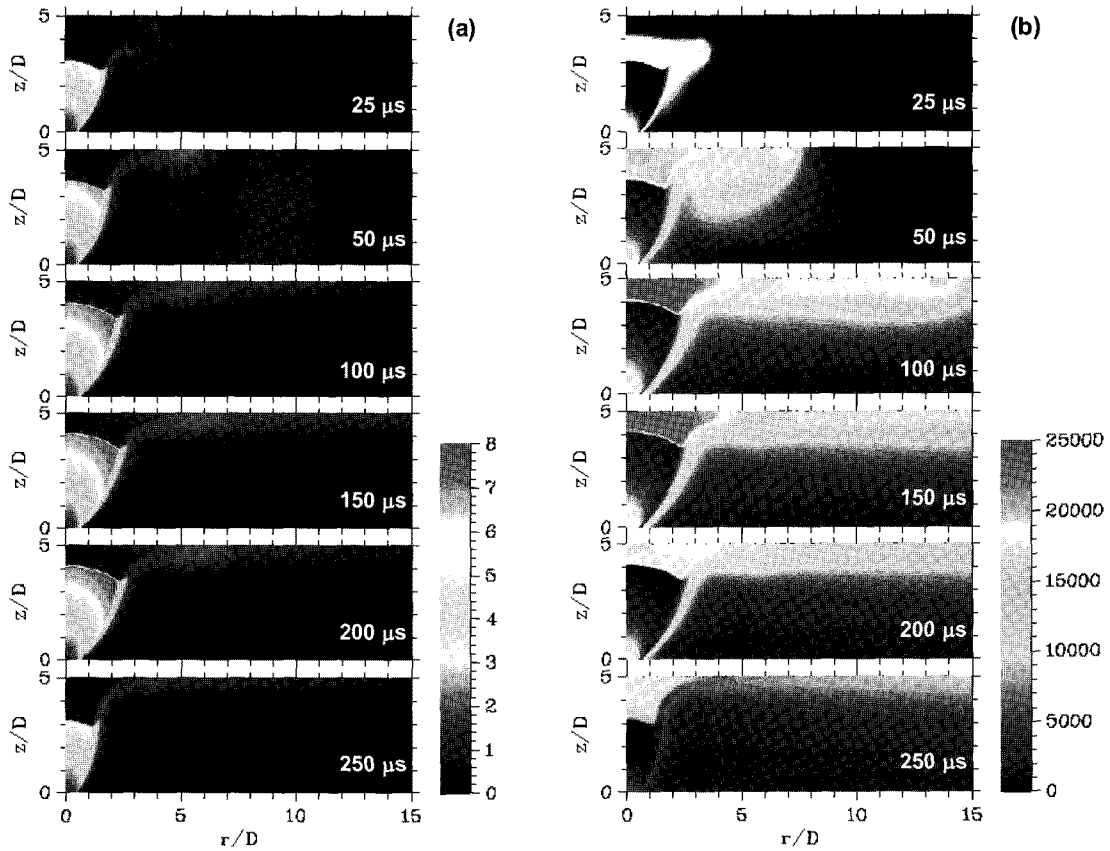

Fig. 5 Transient evolution of (a) Mach number and (b) temperature (in K) contours for the case of L/D = 5

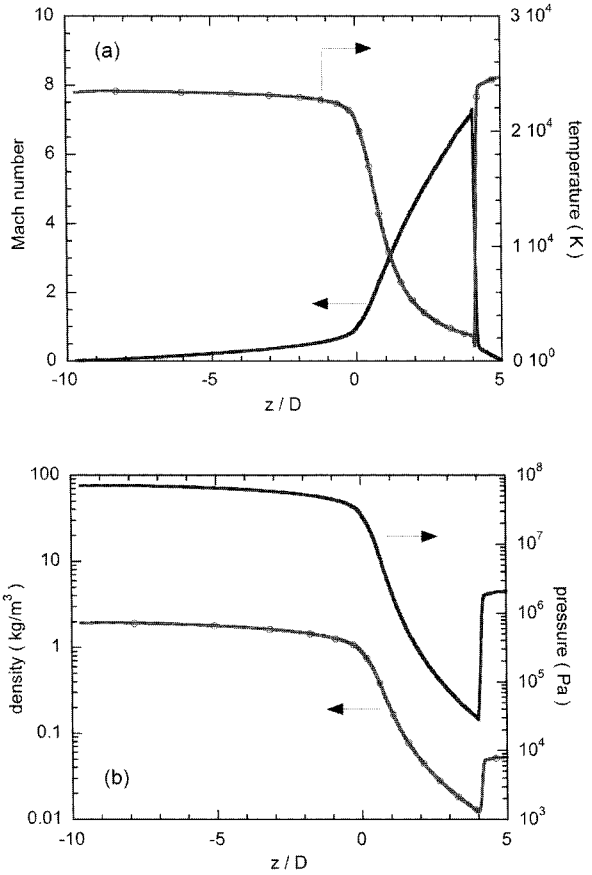

Fig. 6 Plasma (a) Mach number and temperature, (b) pressure and density along the centerline at the time of 125 μs for the case of L/D = 5

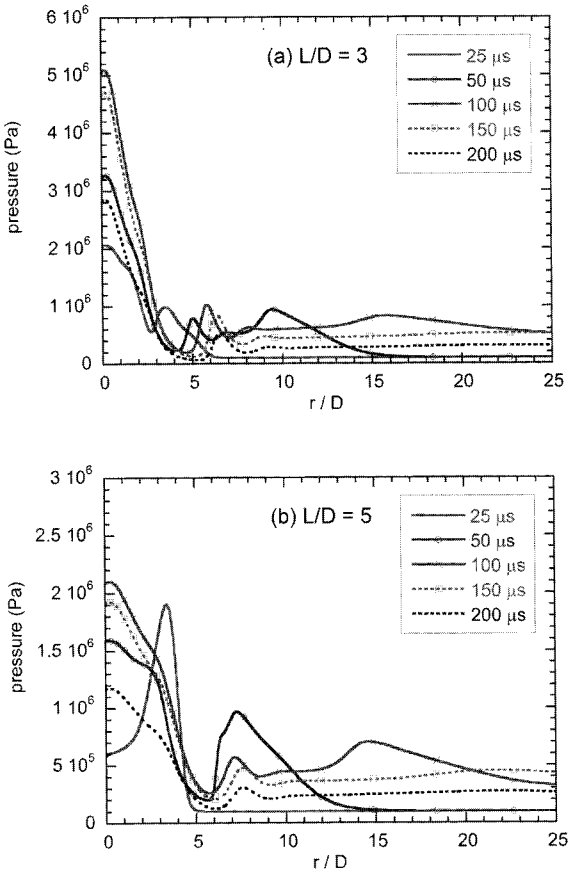

Fig. 7 Temporal change of pressure on the opposing plate surface for the cases of (a) L/D = 3 and (b) L/D = 5

significantly. By numerically integrating the mass ablation density rate, cumulative mass of the bore ablation can be estimated for the entire duration of the plasma firing. In the experiments, capillary bore mass was measured to be approximately 7.6 mg and the calculation yields approximately 9 mg of mass ablation if the blackbody radiation is assumed (f = 1). Deviation factor is found to be 0.85 in order to match the measured mass ablation and this value is used in the calculations shown here as well as in the previous study[11]. No significant change of bore exit conditions or ablated bore mass with the presence and the variation of opposing plate location is found in comparison between two cases of present computations and the case of the open-air discharge and it is due to the flow choking at the bore exit (M = 1).

Figs. 4 and 5 present the transient evolution of Mach number and temperature contours of plasma flow for two cases of L/D = 3 and 5 at six time steps during the pulsed plasma discharge. In those figures, the location of r/D = 0 and z/D = 0 is the center of bore exit. Mach number is evaluated based on the following equation of speed of sound.

$$c_s = \sqrt{\gamma_{eff}(1+\alpha)R_h T} \tag{12}$$

where R_h is the average gas constant of heavy species and the effective specific heat ratio γ_{eff} is evaluated as

$$\gamma_{eff} = 1 + \frac{P}{\rho e} \tag{13}$$

using the ideal gas approximation. Mach number contours reveal the typical flow pattern of a highly underexpanded supersonic jet featuring strong Mach disk and the barrel

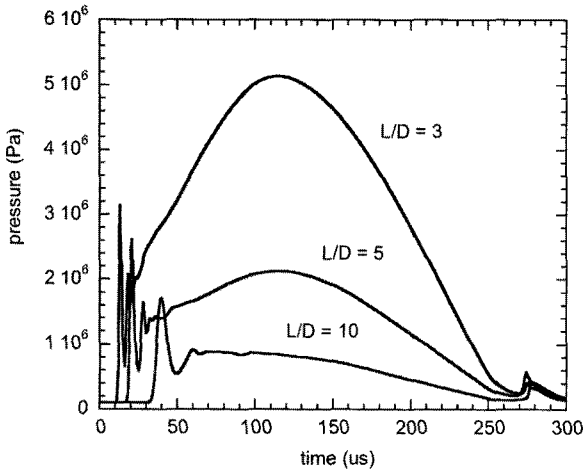

Fig. 8 Temporal change of stagnation point pressure on the opposing plate surface for the cases of L/D = 3, 5 and 10

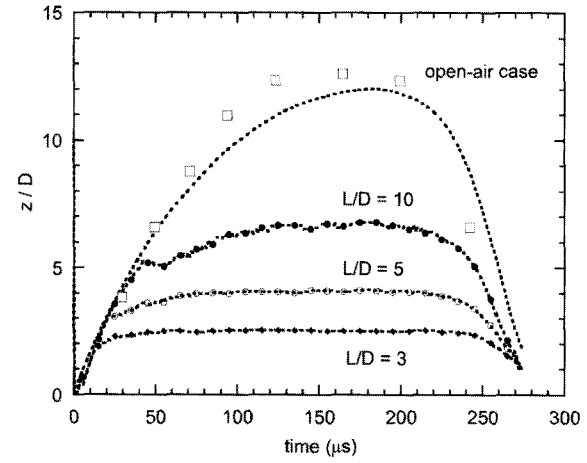

Fig. 9 Temporal location of Mach disk at the centerline during the plasma discharge for the cases of different distance between the bore exit and the opposing plate. Symbols represent the measured data for the open-air case[7]

shock. Also at the time of 25 μs, propagation of the hemispherical blast wave can be observed in both cases. The contact surface between the plasma and the background gas can be identified in temperature contours and the vortex flow motion around the upper right tip of the evolving shock. In both cases of L/D, the plasma discharge starts interacting with the opposing plate before the time of 25 μs.

Fig. 6 shows the plasma flow Mach number, temperature, pressure, and density along the centerline at the time of 125 μs for the case of L/D = 5. Inside the capillary bore (z/D < 0), plasma temperature, density, and pressure do not vary significantly to the axial direction, while the Mach number reaches unity at the bore exit (z/D = 0). However, the outside the capillary bore (z/D > 0), the flow conditions undergo significant variation from the bore exit to the stagnation point on the plate. Shock expansion and the location of Mach disk can be seen at z/D ≈ 4.

Temporal change of pressure on the surface of opposing plate is shown in Fig. 7(a) and (b) for the case of L/D = 3 and 5, respectively. As expected, the magnitude of pressure level is significantly higher in the case of L/D = 3, although there are similar pattern of change in both cases. Time change of pressure at the stagnation point on the plate is shown in Fig. 8 for three cases of L/D = 3, 5, and 10. At the early time stages, those sharp peaks of pressure represent the arrival of the blast wave propagation, which reflection by the surface interacts with the main shock that comes later in time. In the case that the plate is closest to the bore exit (L/D = 3), the maximum pressure at the stagnation point reaches approximately 5 MPa. However, the plate distance increases, the pressure level at the stagnation point decreases significantly.

Mach disk location of the evolving and devolving shock is shown in Fig. 9 for three cases of L/D, and compared with the case of open-air plasma discharge without the presence of the opposing plate. In the figure, the symbols represent the experimental data from the visible emission measurements[7] and the dotted line are the computational results of free jet from the previous study[11]. When the plasma discharge is shot without the opposing plate, the Mach disk extends up to approximately 12 bore diameters from the bore exit. However, the present cases of impinging plasma jet show the limited expansion of shock structure and the maximum Mach disk location is 84, 83, and 68 percent of the spacing between the bore exit and the opposing plate for the cases of L/D = 3, 5, and 10, respectively. The shock evolution tends to become more quasi-steady when the opposing plate is closer to the bore exit.

4. CONCLUSIONS

The pulsed plasma discharge from the electrothermal gun impinging on a flat surface has been numerically investigated by utilizing the time-dependent inviscid gas dynamics equations with the FCT computational algorithm for the two-dimensional axisymmetric computational

domain. A change of distance between the bore exit and the opposing plate does not significantly modify the flow conditions inside the capillary bore due to the choking at the bore exit. The impingement of plasma discharge shows the shock characteristics of the highly underexpanded jet and the computational results are displayed to show the effect of the distance between the capillary bore and the opposing surface on the time-changing shock structure including contact surface, Mach disk, and blast wave propagation.

ACKNOWLEDGEMENT

This research was supported by Research Fund, Kumoh National Institute of Technology.

REFERENCES

[1] 1993, Tidman, D.A. and Massey, D.W., "Electrothermal Light Gas Gun," *IEEE Trans. Magn.*, Vol.29, pp.621-624.

[2] 1997, White, K.J., Katulka, G.L., Khong, T. and Nekula, K., "Plasma Characterization for Electrothermal-Chemical Gun Applications," *ARL-TR-1491,* U.S. Army Research Laboratory, Aberdeen Proving Ground.

[3] 1999, Nusca, M.J., White, K.J., Williams, A.W., Landsberg, A.M., Young, T.R. and Lind, C.A., "Computational and Experimental Investigations of Open-Air Plasma Discharges," *AIAA Paper 99-0865.*

[4] 2008, Pekker, L., "A Zero Dimensional Time-Dependent Model of High Pressure Ablative Capillary Discharge," *AIAA Paper 2008-3891.*

[5] 1997, Peterson, D.R., "Design and Operation of the Electrogun, an Electrothermal Gun for Producing Metal and Carbon Plasma Jets," *IEEE Trans. Magn.*, Vol.33, pp.373-378.

[6] 2008, Kim, K. and Peterson, D.R., "A Low Aspect Ratio Electrothermal Gun for Metal Plasma Vapor Discharge and Ceramic Nanopowder Production," *J. Mech. Sci. Technol.*, Vol.22, pp.1408-1416.

[7] 1997, Kohel, J.M., Su, L.K., Clemens, N.T. and Varghese, P.L., "Emission Spectroscopic Measurements and Analysis of a Pulsed Plasma Jet," *IEEE Trans. Magn.*, Vol.35, pp.201-206.

[8] 1992, Powell, J.D. and Zielinski, A.E., "Theory and Experiment for an Ablating-Capillary Discharge and Applications to Electrothermal-Chemical Guns," *BRL-TR-3355,* U.S. Army Ballistic Research Laboratory, Aberdeen Proving Ground.

[9] 2001, Zaghloul, M.F., Bourham, M.A. and Doster, J.M., "Semi-Analytical Modelling and Simulation of the Evolution and Flow of Ohmically-Heated Non-Ideal Plasmas in Electrothermal Guns," *J. Phys. D: Appl. Phys.*, Vol.34, pp.772-786.

[10] 2003, Kim, K., "Time-Dependent One-Dimensional Modeling of Pulsed Plasma Discharge in a Capillary Plasma Device," *IEEE Trans. Plasma Sci.*, Vol.31, pp.729-735.

[11] 2008, Kim, K., "Transient Flowfield Characteristics of Polycarbonate Plasma Discharge from Pulse-Powered Electrothermal Gun Operation," *J. Therm. Spray Technol.*, Vol.17, pp.517-524.

[12] 1975, Schmidt, E.M. and Shear, D.D., "Optical Measurements of Muzzle Blast," *AIAA J.*, Vol.13, pp.1086-1091.

[13] 1987, Liebermann, R.W. and Zollweg, R.J., "Electrical Conductivity of Nonideal Plasmas," *J. Appl. Phys.*, Vol.62, pp.3621-3627.

[14] 1995, Batteh, J., Powell, J., Sink, D. and Thornhill, L., "A Methodology for Computing Thermodynamic and Transport Properties of Plasma Mixtures in ETC Injectors," *IEEE Trans. Magn.*, Vol.31, pp.388-393.

[15] 1993, Boris, J.P., Landsberg, A.M., Oran, E.S. and Gardner, J.H., "LCPFCT - Flux-Corrected Transport Algorithm for Solving Generalized Continuity Equations," *NRL MR 6410-93-7192,* Naval Research Laboratory, Washington, D.C.

[16] 1976, Boris, J.P., "Flux-Corrected Transport Modules for Generalized Continuity Equations," *NRL MR 3237,* Naval Research Laboratory, Washington, D.C.